Effect of Periodic Background Loss on Grating Spectra

Vittoria Finazzi and Mikhail N. Zervas
Optoelectronics Research Centre, Southampton University, Southampton, SO17 1BJ, UK

(Dated: December 19, 2000)

Abstract

The effect of periodic loss on the performance of refractive-index gratings has been studied in detail. It is shown that the loss periodicity and relative phase strongly affects the symmetry of the reflection, transmission and loss spectra. This asymmetry has been successfully explained by considering the overlap between the standing-wave intensity distribution and periodic loss pattern.

Submitted to "Journal of Applied Optics"

grating structures [8], which rely on the differential electric-field/gain-medium overlap to reduce the gain threshold of one of the spatial modes.

The FBG writing process involves side-illumination of the fibre with a periodic UV radiation pattern [9]. In addition to the induced refractive index changes, UV illumination increases the propagation background losses around 1550 nm. The level of background losses depends on the fibre type, photosensitization process and writing conditions.

For a hydrogen-loaded fibre (3mol% H_2) exposed to uniform UV light at 244 nm, the measured average background loss at 1550nm was 0.2 dB/cm [10]. This average loss is known to scale with the UV fluence and therefore with the induced refractive index change [11]. It is, therefore, expected that exposure to periodically varying UV intensity, in addition to periodic refractive index change, will result in a periodic modulation of the induced background loss. It should also be stressed that depending on the way it is introduced, the periodic loss can be in-phase or anti-phase with the periodic refractive index pattern.

Combined metal/dielectric periodic layers are also used as photonic band gap structures to produce optical filters with enhanced transmissivity at various wavelengths ranges [12, 13]. These filters rely again on the presence of the periodic loss to selectively suppress certain transmission windows.

Refractive index (photorefractive) gratings and loss (photochromic) gratings are also known to coexist in various photorefractive materials [14–17]. Photorefractive and photochromic gratings are spatially separated by some spatial phase ϕ, which depends on the physical mechanisms of charge transport and charge trapping, the grating writing conditions and material properties. The spatial phase ϕ affects the overall coupling process and diffraction data and may lead to erroneous conclusions.

In this paper, we consider and analyse thoroughly the effect of the periodic modulated background loss on the spectral response of FBGs. The theoretical study is achieved by extending the standard coupled-mode theory (CMT) to include the effect of periodic loss. It is shown that, as in the case of the localised scattering centre [4], the grating spectrum is affected non-uniformly by the presence of the periodic loss. In section II, we develop

where $\beta_0 = k_0 n$ and

$$\kappa_c = \frac{\pi}{\lambda} n_1 + j\frac{\alpha_1}{2}\cos\phi \tag{5a}$$

$$\kappa_s = j\frac{\alpha_1}{2}\sin\phi \tag{5b}$$

are the expressions of the extended coupling constants. When the Bragg scattering dominates ($\beta_0 \approx \beta_B$), the wave equation

$$\nabla^2 E + k^2(z)E(z) = 0 \tag{6}$$

can be analytically solved, because only two of the infinite set of diffraction orders are in phase and have significant amplitude. So the total electric field can be written as the sum of two counter-propagating waves of complex amplitudes $A(z)$ and $B(z)$, respectively, namely

$$E(z) = E_f(z) + E_b(z) = A(z)e^{j\beta z} + B(z)e^{-j\beta z} \tag{7}$$

where β is the propagation constant of the uncoupled waves ($n_1, \alpha_1 = 0$) defined as

$$\beta^2 = (\beta_0 + j\alpha)^2 \approx \beta_0^2 + j2\beta_0\alpha. \tag{8}$$

Substituting (7) into the wave equation (6), equating synchronous terms and using the slowly-varying envelope approximation [18], the following pair of coupled-wave equations can be obtained:

$$\begin{cases} \dfrac{\partial A}{\partial z} = j(\kappa_c + j\kappa_s)e^{j2\Delta z}B \\ \\ \dfrac{\partial B}{\partial z} = -j(\kappa_c - j\kappa_s)e^{-j2\Delta z}A \end{cases} \tag{9}$$

with $\Delta \equiv \beta_B - \beta = \beta_B - \beta_0 - j\alpha$. The integration of the system (9), with boundary conditions $E_b(L) = 0$ and $E_f(0) = E_{inc}$, leads to the following expressions of the forward and backward components of the electric field

$$E_f(z) = E_{inc}\frac{p\cosh(p(z-L)) - j\Delta\sinh(p(z-L))}{p\cosh(pL) + j\Delta\sinh(pL)}e^{j\beta_B z} \tag{10a}$$

$$E_b(z) = -jE_{inc}\frac{(\kappa_c - j\kappa_s)\sinh(p(z-L))}{p\cosh(pL) + j\Delta\sinh(pL)}e^{-j\beta_B z}. \tag{10b}$$

of the amplitude and relative spatial phase of the loss grating on the obtained reflectivity and loss spectra is studied in detail. The physical insight on the resulting spectra is also provided.

Figure 2 shows the spectral characteristics of a uniform-loss grating with $n = 1.45$, $n_1 = 10^{-4}$, $L = 2$ cm, $\lambda_B = 1550$ nm, $\alpha = 0.023$ cm^{-1} and $\alpha_1 = 0$. This value of α corresponds to the power loss coefficient $\alpha_p = 0.2$ dB/cm that has been experimentally measured in [10], for an hydrogen loaded (3mol% H_2) germanosilicate fibre (through the relation $\alpha[\text{cm}^{-1}] = (1/20)\ln 10 \cdot \alpha_p[\text{dB/cm}]$). All the curves are plotted as a function of the wavelength detuning $\Delta\lambda = \lambda - \lambda_B$. The lossless case ($\alpha = 0$, dashed line) is also plotted for comparison. Figures 2(a) and (b) show the reflectivity and transmissivity spectra. It is confirmed that the uniform background loss reduces both the grating reflectivity and transmissivity. The latter results in an increased device insertion loss. The effect is most severe around the wavelengths of maximum transmission at the edges of the stop-band. Figures 2(c) and (d) show the spectra of the phase-time delay of the reflected and transmitted light, calculated by using (14). It is shown that the presence of uniform background loss breaks the time-delay degeneracy between reflected and transmitted light that otherwise exists in lossless one-dimensional band gap structures. The phase-time delay (especially of the transmitted light) is reduced considerably around the stop-band edges, as marked in Figure 2(d). This is equivalent to the reduction of the Q factor of resonant cavities, e.g. Fabry-Perot interferometer, in the presence of intra-cavity losses (after all, Bragg gratings *are* distributed resonant cavities). Figure 2(e) shows the corresponding grating total-loss spectrum in the presence of uniform propagation background loss.

It is shown that the loss spectrum is quite non-uniform across the grating bandwidth. The minimum loss occurs at the Bragg wavelength ($\Delta\lambda = 0$), since at this wavelength the incident light is predominantly reflected ($R \gg T$) without penetrating deep into the lossy grating structure. The penetration depth is inversely proportional to the grating strength [21] and, therefore, the minimum loss decreases with the grating reflectivity. The maximum loss, on the other hand, is shown to occur at the edges of the stop-band. At

modulation, despite the spatial symmetry, the response of a grating is clearly *asymmetric*.

This asymmetry is further demonstrated in Figure 4 where the differences in reflectivity (a), equivalent time delay (b) and total loss (c), between the periodic (with ϕ=0) and uniform background loss cases, are plotted as a function of the wavelength detuning. The grating parameters are the same as the ones in Figures 2 and 3. Despite the fact that the average propagation loss coefficient is equal in both cases ($\alpha = 0.023$ cm^{-1}), the total loss in the periodic case is larger ($\Delta\alpha_{\text{loss}} > 0$) than the uniform one at the long-wavelength side ($\Delta\lambda > 0$). The opposite is true at the short-wavelength side ($\Delta\lambda < 0$). It is also shown that the part of the spectrum experiencing higher (lower) losses is also associated with lower (higher) reflectivity and time delay.

The origin of the asymmetry in the grating response, in the presence of periodic loss, can be understood by considering the dispersive nature of the grating structure and its effect on the total field intensity distribution along the grating. Figure 5 shows the total electric-field intensity distribution (solid line) for five different wavelengths in five different grating regions. The shaded area shows the corresponding refractive-index modulation in each region. To better visualise the spatial dephasing between the two patterns, the total field intensity in each region is expressed in arbitrary units. Each column corresponds to the same location along the grating, specified by the z-coordinate shown on the top, while each row corresponds to the same wavelength, indicated at the far left. λ_{B} is the Bragg wavelength, while λ_{I}^{+} and λ_{II}^{+} correspond to the resonant wavelengths at the first and second reflectivity zero ($R = 0$, $T = 1$), respectively, at the long-wavelength side of the spectrum (the superscript $(-)$ denotes the corresponding wavelengths at the short-wavelength side). Each grating subregion is 5-period long.

For all wavelengths, the spatial dephasing at the grating far end ($z = L$) is equal to $-\pi/2$ (see Appendix A). This is due to the boundary condition at $z = L$ and the nature of the elementary partial standing-wave pattern formed by the last refractive-index-modulation fringe. Inside the grating, however, the spatial dephasing depends strongly on the wavelength and the relative grating position. For example, the total-field-intensity periodic pattern at

(c.f., $\lambda_{\rm I}^{+}$ and $\lambda_{\rm II}^{+}$) the high-intensity fringes are predominantly aligned with the high-loss ones and it is expected to impart maximum loss. In the short-wavelength side (c.f., $\lambda_{\rm I}^{-}$ and $\lambda_{\rm II}^{-}$) the high-intensity fringes are predominantly aligned with the low-loss ones and it is, therefore, expected to impart minimum loss. This also explains why the short-wavelength total loss for the modulated case is even lower than the corresponding value for the equivalent uniform one (see Fig. 4(c)).

The effect of the dephasing factor ϕ between the refractive index and loss modulation on the total loss spectrum is illustrated in Figure 7. The grating parameters are similar to the ones in Figure 3 and $\phi = 0$, $\pi/2$, π and $3\pi/2$. The corresponding reflectivity spectra are shown in Figure 8, where the peak has been magnified in the inset. It is first shown that the $\phi = \pi$ case (dashed line) is a mirror image of the corresponding $\phi = 0$ one (solid line). This is due to the fact that by shifting the modulated loss pattern by π with respect to the modulated index pattern, the overlaps between the intensity pattern (which is determined by the index modulation and, therefore, remains unchanged) and the loss pattern is now maximised in the short wavelength side. At the Bragg wavelength, due to resulting spatial symmetry, the $\phi = 0$ and $\phi = \pi$ cases give the same response (equal to the uniform loss case). This is further demonstrated in Figure 9, where the total intensity distribution at the Bragg wavelength (thick solid line), refractive index variation (thin solid line) and loss modulation (shaded area) are plotted over five grating periods, for $\phi = 0$, $\pi/2$, π and $3\pi/2$. For $\phi = \pi/2$ and $3\pi/2$, although the reflectivity and loss spectra become symmetric with respect to wavelength detuning, they acquire different peak values at the Bragg wavelength. In fact, the $\phi = \pi/2$ case (dot-dashed line) shows smaller loss and higher reflectivity compared to $\phi = 3\pi/2$ case (dot-dot-dashed line). It also appears that the uniform-loss case (dotted line) performance corresponds to the average of the $\phi = \pi/2$ and $3\pi/2$ cases. This is again related to the spatial relation between the corresponding field-intensity and modulated-loss patterns (c.f., Fig. 9(b) and (d)). Spatial shifts of $\phi = \pi/2$ and $3\pi/2$ align the field-intensity maxima with the modulated-loss minima and maxima, respectively.

Background loss (uniform or modulated) not only affects the reflectivity and time-delay

weak gratings the resonance effects at the edges of the stop band are very small and the loss peaks diminish. For this reason the four plots have different starting points. As the value of the loss α_p is increased, the maximum position shifts to a higher n_1 value because a stronger value of the index coupling coefficient is required to overcome that particular loss grating.

Secondly, we consider the performance of gratings with fixed length when both the refractive index modulation and loss modulation amplitudes increase proportionally (fixed α/n_1 ratio). This is a situation most likely to be encountered in practice when the UV writing process introduces additional losses [11]. Figure 13(a) shows the variation of $\Delta\alpha_{\text{peaks}}$ as a function of the refractive index modulation amplitude, and for $L = 2$ cm, a fully modulated background loss with $\phi = 0$ and five different values of the ratio α/n_1. The value of α_p at $n_1 = 3 \cdot 10^{-4}$ is equal to 0.3 dB/cm (solid line), 0.2 dB/cm (long dashed line), 0.1 dB/cm (medium dashed line), 0.05 dB/cm (short dashed line) and 0.01 dB/cm (dotted line). As the index modulation increases, the function $\Delta\alpha_{\text{peaks}}$, after an initial increase, decreases again. Now the index/loss coupling coefficients grow proportionally, but the average value of the loss is always increased. Due to the spectrum asymmetry the reflectivity peak shifts to a wavelength λ_p shorter than λ_B. The wavelength shift $|\lambda_p - \lambda_B|$ is plotted in Figure 13(b), while in Figure 13(c) the shift has been normalized to the peaks difference $\Delta\lambda_{\text{peaks}}$, proportional to the grating spectral bandwidth. However, this shift is a very small proportion of the total band gap.

IV. CONCLUSIONS

In the first section of this work has been reported the analytical solution of the wave equation considering a loss medium with a periodic modulation of both the real and imaginary part of the refractive index. For the sake of generality a dephasing factor ϕ has been considered between the two patterns. The expressions for the fields distribution along the grating length and for the reflection and transmission coefficients have been determined. In the second section the simulation results obtained with the help of these expressions are

(A2) describes a generalised standing-wave pattern with local fringe contrast:

$$F(z) = \frac{2\,|A(z)|\,|B(z)|}{|A(z)|^2 + |B(z)|^2} = \frac{2\,|E_f(z)|\,|E_b(z)|}{|E_f(z)|^2 + |E_b(z)|^2}. \tag{A3}$$

The fringe contrast will vary along the grating length. The local period of the standing wave (Λ_{sw}) is determined by the total spatial phase of Equation (A2) as follows:

$$\Phi(z) = 2\beta z + \Delta\phi_{\mathrm{AB}} = \int_0^z \frac{2\pi}{\Lambda_{sw}(\zeta)} d\zeta \tag{A4}$$

from which we obtain:

$$\frac{2\pi}{\Lambda_{sw}(z)} = \frac{d\Phi(z)}{dz} = 2\beta + \frac{d\phi_{\mathrm{A}}(z)}{dz} - \frac{d\phi_{\mathrm{B}}(z)}{dz}. \tag{A5}$$

Under the SVEA, $d\phi_{\mathrm{A}}/dz \approx d\phi_{\mathrm{B}}/dz \approx 0$ and, therefore,

$$\Lambda_{sw} = \frac{\lambda}{2n} = \frac{\lambda_n}{2} \tag{A6}$$

where $\lambda_n = \lambda/n$ is the optical wavelength in the propagation medium with refractive index n. The standing wave period is constant along the entire grating length and is proportional to the optical wavelength of the incident wave. It is, therefore, expected that there will be a spatial dephasing between the standing-wave and refractive-index periodic patterns that depends on the incident optical wavelength.

The spatial dephasing can be determined by starting from the full expressions for $E_f(z)$ and $E_b(z)$ given by Equations (10). Expressing the forward- and backward-propagating electric fields as $E_f(z) = |E_f(z)|\exp[j\phi_f(z)]\exp(j\beta_{\mathrm{B}}z)$ and $E_b(z) = |E_b(z)|\exp[j\phi_b(z)]\exp(-j\beta_{\mathrm{B}}z)$, the total electric-field intensity can be re-written as:

$$I(z) = |E(z)|^2 = |E_f(z)|^2 + |E_b(z)|^2 + 2\,|E_f(z)|\,|E_b(z)|\cos\big(2\beta_{\mathrm{B}}z + \Delta\phi_{fb}(z)\big). \tag{A7}$$

The standing-wave pattern is now expressed in terms of the grating spatial phase $2\beta_{\mathrm{B}}z$ (c.f. Eqn. (1a)). The term $\Delta\phi_{fb} = \phi_f(z) - \phi_b(z)$ gives, therefore, directly the spatial dephasing between the total field intensity and the fixed periodic refractive-index modulation, at any point within the grating. In the following analysis of $\Delta\phi_{fb}$ it may be helpful to refer to Figure 6 for some of the discussed issues.

the higher (z_m^+) or lower (z_m^-) values, from (A9) we can derive that

$$\phi_f^{\pm}(z_m^+) = \mp\bar{p}L + m\pi \tag{A10a}$$

$$\phi_b^{\pm}(z_m^+) = \mp\frac{\pi}{2} \mp \bar{p}L + \binom{m+1}{m}\pi \tag{A10b}$$

and

$$\phi_f^{\pm}(z_m^-) = \mp\bar{p}L + m\pi \tag{A10c}$$

$$\phi_b^{\pm}(z_m^-) = \mp\frac{\pi}{2} \mp \bar{p}L + \binom{m}{m+1}\pi \tag{A10d}$$

where the upper (lower) part is valid for the long (short) wavelength side. It is now easily deduced that, independently from the wavelength side, $\Delta\phi_{fb}(z_m^+) = +\pi/2$ and $\Delta\phi_{fb}(z_m^-) = -\pi/2$. So at z_m precisely, the local dephasing shows a π phase discontinuity.

The local dephasing at the midpoint $\bar{z}_m$ between two consecutive field nodes z_m and z_{m+1} depends instead on the wavelength side. From Equations (A9) the expressions of ϕ_f and ϕ_b at $\bar{z}_m = (z_m + z_{m+1})/2 = L - (2m+1)\pi/2\bar{p}$ can be written as

$$\phi_f^{\pm}(\bar{z}_m) = \mp\bar{p}L \pm \frac{(2m+1)\pi}{2} \tag{A11a}$$

$$\phi_b^{\pm}(\bar{z}_m) = \pm\left(\frac{\pi}{2} - \bar{p}L\right) + \binom{m}{m+1}\pi. \tag{A11b}$$

For the short-wavelength side $\Delta\phi_{fb}^-(\bar{z}_m) = \pi$, while for the long-wavelength one $\Delta\phi_{fb}^+(\bar{z}_m) = 0$.

We now consider the spectral region inside the band-gap where $\Delta^2 < \kappa^2$, $p = \sqrt{\kappa^2 - \Delta^2}$ is real and we obtain

$$\phi_f(z) = \arctan\left(\frac{-2p\Delta\sinh pz}{(p^2-\Delta^2)\cosh pz + \kappa^2\cosh p(z-2L)}\right) \tag{A12a}$$

$$\phi_b(z) = \arctan\left(\frac{p}{\Delta}\coth pL\right) + \pi\hat{\delta}(\Delta < 0). \tag{A12b}$$

Since the denominator of the arctangent argument of ϕ_f is always positive, its sign is determined by the numerator, so that $\phi_f^+ = -\phi_f^-$ is verified. For ϕ_b the justification used for (A8b) can be repeated, so $\phi_b^+ = -\phi_b^- + \pi$ and $\Delta\phi_{fb}^+ = -\Delta\phi_{fb}^- + \pi$. Moreover, the π shift

where the background-loss perturbation is given by Equation (1b).

Expressing the total electric-field intensity as in Equation (A7), under the SVEA the integral (B2) can be simplified as

$$I_{\text{loss}}(\lambda) \approx \frac{2\alpha}{|E_{\text{inc}}|^2}\int_0^L (|E_f(z,\lambda)|^2 + |E_b(z,\lambda)|^2)dz + \frac{2\alpha_1}{|E_{\text{inc}}|^2}\int_0^L |E_f(z,\lambda)|\,|E_b(z,\lambda)|\cos(\phi - \Delta\phi_{fb}(z,\lambda))dz. \quad \text{(B3a)}$$

In the cases considered in this work, the integral (B3) gives the same loss spectrum obtained as $I_{\text{loss}} = 1 - R - T$. Studying the wavelength dependence of $|E_f(z,\lambda)|$, $|E_b(z,\lambda)|$, and $\Delta\phi_{fb}(z,\lambda)$, it is possible to give an alternative explanation to the symmetric/anti-symmetric behaviour of the grating loss spectrum for the different values of the dephasing factor ϕ. Since the moduli of the forward- and backward-propagating fields are symmetric with respect to the Bragg wavelength, the first term in (B3), that is ϕ-independent, is also symmetric with respect to λ_B. The asymmetry observed for $\phi = 0$ and π is then due to the second term in (B3), in particularly to the fact that $\Delta\phi_{fb}(z,\lambda^+) = -\Delta\phi_{fb}(z,\lambda^-) + \pi$, as demonstrated in the Appendix A.

[20] T. Erdogan, J. Lightwave Technol. **15**(8), 1277 (1997).

[21] D. I. Babic and S. W. Corzine, IEEE J. Quantum Electron. **28**(2), 514 (1992).

[22] A. W. Snyder and J. D. Love, *Optical waveguide theory* (Chapman and Hall, 1983).

7 Spectral loss (dB) as a function of the wavelength detuning (nm) for different dephasing angles: (a) $\phi = 0$ in solid and $\phi = \pi$ in dashed line; (b) $\phi = \pi/2$ in dot-dashed and $\phi = 3\pi/2$ in dot-dot-dashed line; the uniform-loss case is also shown in dotted line. All the other parameters are as in Fig 3. The straight dotted line, that appears in both (a) and (b), represents the average single-pass loss level. 31

8 Reflectivity spectra versus wavelength detuning corresponding to the four full modulated-loss and the uniform-loss cases illustrated in Fig. 7. The reflectivity peak has been magnified in the inset. 32

9 Intensity distribution (thick line), refractive index pattern (thin line) and background loss pattern (shaded area) versus grating length over five periods, at the Bragg wavelength and for a dephasing angle equal to: (a) $\phi = 0$, (b) $\phi = \pi/2$, (c) $\phi = \pi$, (d) $\phi = 3\pi/2$ (the three quantities are expressed in arbitrary units). 33

10 Reflectivity peak R_B versus κL for: $n_1 = 10^{-3}$ (upper curve), $n_1 = 10^{-4}$ (middle curve), $n_1 = 10^{-5}$ (lower curve); $\alpha_p = 0.2$ dB/cm, $\alpha_1 = 0$ (uniform loss); κ is the real part of κ_c. 34

11 Reflectivity peak R_B versus κL for four ϕ values (solid lines), with $n_1 = 10^{-5}$, $\alpha_p = 0.2$ dB/cm, $\alpha_1 = \alpha$ (fully modulated loss); the dotted line corresponds to the lossless case ($\alpha = 0$); κ is the real part of κ_c. 35

12 Amplitude difference $\Delta\alpha_{peaks}$ of the two loss peaks (shown in the inset) as a function of the refractive index modulation, for a (lossless) grating reflectivity of 0.999, $\phi = 0$ and for four different values of the power loss coefficient: $\alpha_p =$ 0.1 dB/cm (solid line), $\alpha_p = 0.2$ dB/cm (long dashed line), $\alpha_p = 0.3$ dB/cm (medium dashed line), $\alpha_p = 0.4$ dB/cm (short dashed line). 36

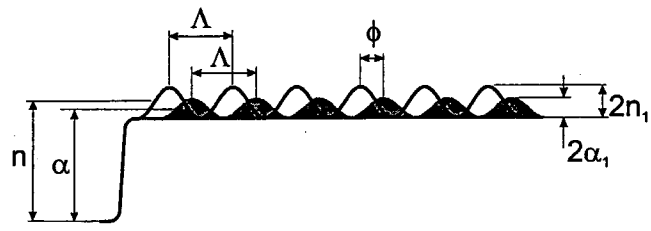

FIG. 1: V. Finazzi, Journal of Applied Physics

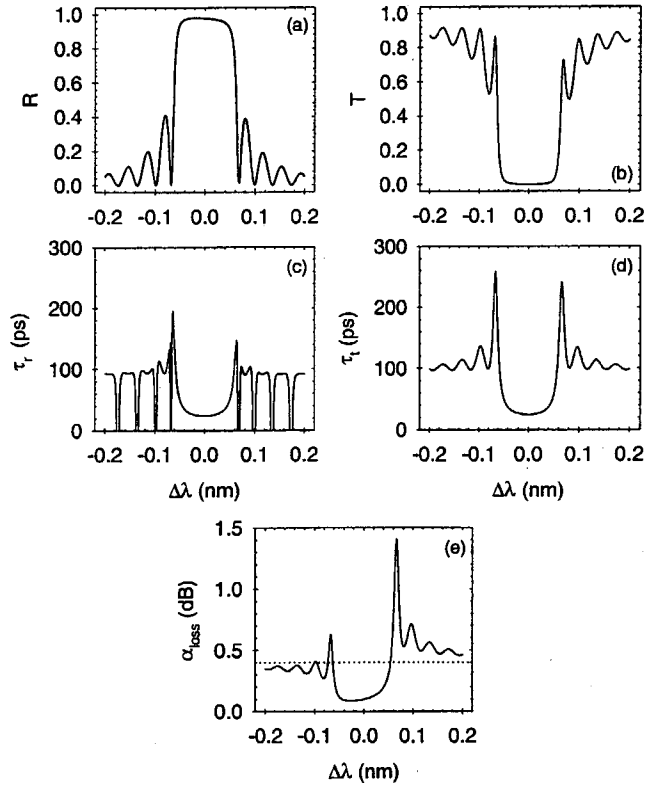

FIG. 3: V. Finazzi, Journal of Applied Physics

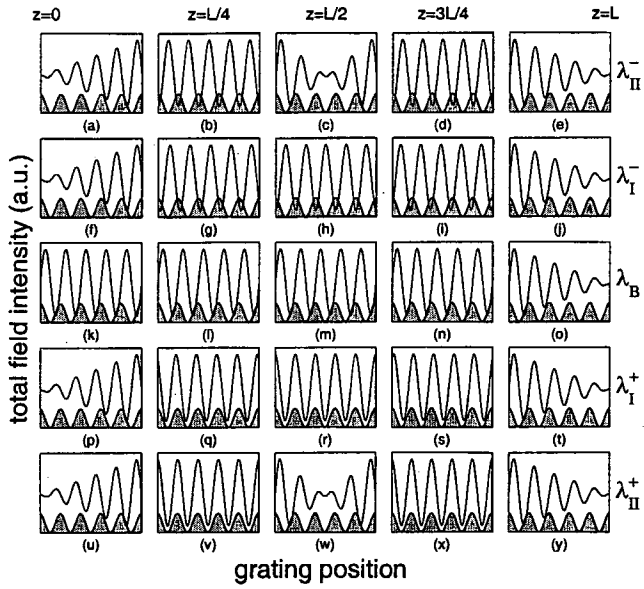

FIG. 5: V. Finazzi, Journal of Applied Physics

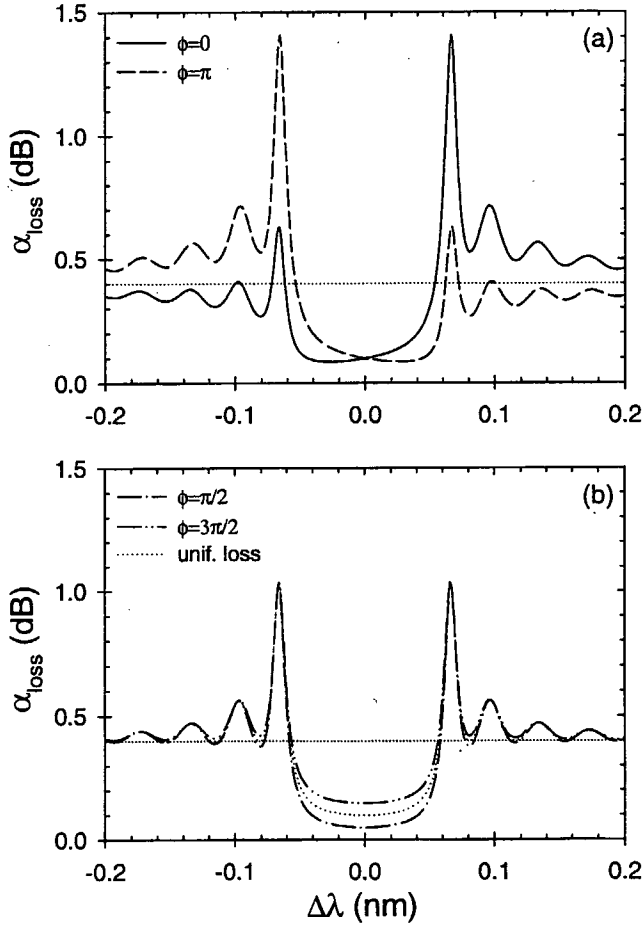

FIG. 7: V. Finazzi, Journal of Applied Physics

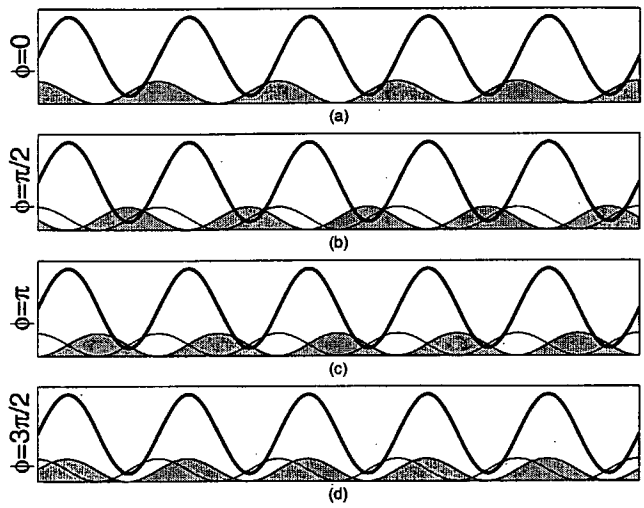

FIG. 9: V. Finazzi, Journal of Applied Physics

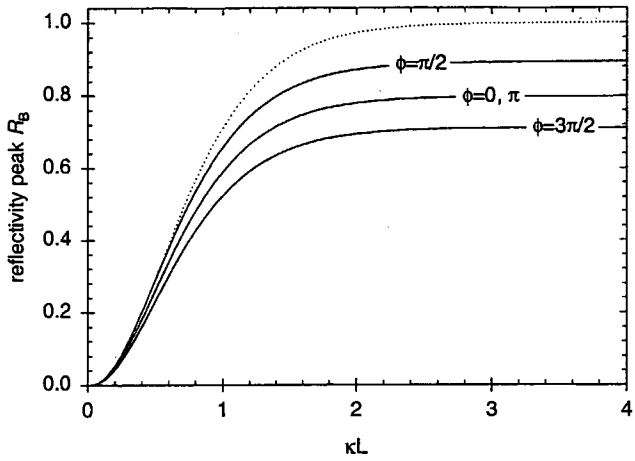

FIG. 11: V. Finazzi, Journal of Applied Physics

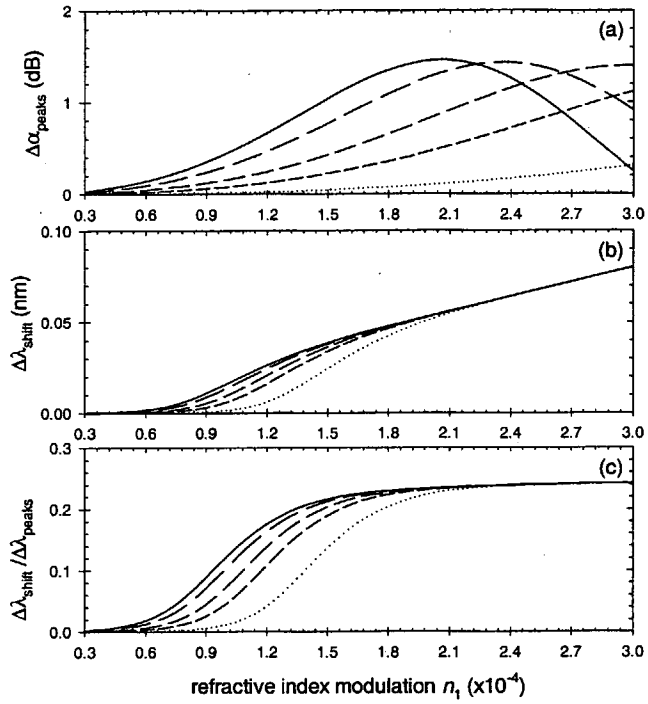

FIG. 13: V. Finazzi, Journal of Applied Physics